ESAIM : Proceedings, Vol. 7, 1999, 369-377
Third International Workshop on Vortex Flows and Related Numerical Methods
http://www.emath.fr/proc/Vol.7/

Sound Generation by the Interaction of a Vortex Ring with a Rigid Sphere

E. Rivoalen †, S. Huberson †, O.M. Knio‡
†Laboratoire de Mécanique, Université du Havre, BP 540, 76058 Le Havre, France
‡ Department of Mechanical Engineering, The Johns Hopkins University, Baltimore, MD 21218-2686, USA

Abstract

High-Reynolds-number interactions between a vortex ring and a stationary rigid sphere are computed using two Lagrangian particle models. The first is a 3D slender vortex filament scheme which tracks the motion of the filament centerline. The centerline velocity is expressed as the sum of a self-induced velocity and potential velocity added to satisfy potential boundary conditions on the surface of the sphere. The self-induced velocity is computed numerically from the line Biot-Savart integral, which is carefully desingularized so as to provide the correct behavior of the vorticity distribution in the asymptotic thin-core limit. The second model is a particle scheme for the simulation of axisymmetric viscous flow. The scheme is based on discretization of the vorticity field into desingularized vortex elements that are advected in a Lagrangian frame. The velocity of the particles is expressed as the sum of a vortex interaction velocity expressed in terms of a desingularized Biot-Savart law, a potential velocity expressed in terms of the image of vortex elements, and a diffusion velocity. The filament and the particle schemes are applied to compute the passage of axisymmetric vortex rings over a stationary rigid sphere in the high-Reynolds-number limit, and to analyze the far-field sound generated by this interaction. Both models show that as the ring passes over the sphere, its radius increases while its core shrinks due stretching. In the parameter regime considered, the two models yield very close predictions of vortex trajectories and speeds. The filament model indicates that the passage leads to the generation of a pressure spike in the acoustic far-field. Meanwhile, the particle computations reveal that in addition to a pressure spike the far-field sound can also exhibit a substantial high-frequency quadrupole emission. Analysis of the computations reveals that this high-frequency noise emission is due to filamentation within the vortex core. The results also show that the high-frequency quadrupole noise may be dominant, especially when the vortex core is thin and the Mach number is not very small.

1 Introduction

In a wide class of noise applications, interactions between concentrated vortices and solid surfaces frequently play an essential role. These interactions may generally involve a number of complex phenomena, including amplification of multiple instability modes, wave and vortex motion, transition and flow separation. Consequently, it is often useful (if not essential) to consider simplified models which enable a tractable analysis of the flow and acoustic fields.

The present work considers an idealized setting which enables us to implement a variety of physical and computational models and, consequently, perform a critical analysis of the predictions. Specifically, we focus on the co-axial passage of vortex ring over a stationary rigid sphere at high Reynolds number. This setup is motivated by some of our own previous computations [1] which featured a simplified analysis of the far-field sound generated during the interaction of a 3D filament with a rigid sphere. In [1] the effect of the sphere was approximated with a potential flow [2], and viscous effects were restricted to the core of the vortex filament. The evolution of the core

Article published by EDP Sciences and available at http://www.edpsciences.org/proc or http://dx.doi.org/10.1051/proc:1999034

under the combined effects of stretching and viscosity were described using an asymptotic model [3,4,5]. The latter is based on a set of underlying assumptions, which include large Reynolds number, small slenderness ratio, and an axisymmetric leading-order core structure. These assumptions naturally restrict the scope of the model; on the other hand, they enable the implementation of a highly-efficient filament scheme and, consequently, analysis of complicated 3D motions.

One of the limitations of slender filament models concerns the simplified representation of the core vorticity distribution and the assumption that the leading-order core structure remains axisymmetric. As mentioned earlier, this approach accounts for the effects of stretching and diffusion on the leading-order structure; unfortunately, it cannot capture more complex modes of core deformation. Thus, the objectives of the present effort is to analyze the role of core deformations on large-scale vortex motion and on sound generation during the passage of an axisymmetric vortex ring over a rigid sphere. We restrict our attention to the high-Reynolds-number flow limit, and compute the flow using two Lagrangian flow models. The first is the slender filament scheme adapted from [1]; the second is a recently-developed particle scheme for axisymmetric viscous flow [6]. In the particle scheme the core is represented using a large number of elements, so that the evolution of the core vorticity distribution can be accurately represented in the calculations. Consequently, the contribution of core deformation phenomena to large-scale vortex motion and to sound radiation can be analyzed by contrasting the predictions of the slender filament and particle computations.

Below, we first provide a brief outline of the slender filament scheme, and summarize the far-field sound computation. Section 3 then provides a brief summary of the particle method. Results of the computations are discussed in section 4.

2 Slender Filament Model

The slender filament model used in the present work is adapted from previous efforts discussed in [1,2,3,4,7]. Thus, only a brief outline is provided.

In the filament model, the vortex centerline is discretized using a finite number of regularized vortex elements, specified in terms their Lagrangian position vectors, $\chi_i(t)$, $i, \ldots, N$. The elements are indexed consecutively such that the collection $\{\chi_i(t)\}_{i=1}^{N}$ approximates the filament centerline [8]. The elements are transported according to the ring centerline velocity, given by the asymptotic evolution equation:

$$\dot{\boldsymbol{X}}(s) = \boldsymbol{v}^{\mathrm{si}}(s) + \boldsymbol{v}^{\mathrm{out}}(s) \tag{1}$$

where $\boldsymbol{v}^{\mathrm{si}}$ denotes the filament self-induced velocity, and $\boldsymbol{v}^{\mathrm{out}}$ is an outer velocity field [5]. Here, $\boldsymbol{X}$ is the coordinate of the filament centerline and s is the arc length parameter along the centerline. Following [3,4], the self-induced velocity is obtained from the desingularized Biot-Savart law:

$$\boldsymbol{v}^{\mathrm{si}}(\boldsymbol{x},t) = -\frac{\Gamma}{4\pi}\sum_{i=1}^{N}\frac{(\boldsymbol{x}-\chi_i(t))\times\delta\chi_i(t)}{|\boldsymbol{x}-\chi_i(t)|^3}\kappa_\delta(\boldsymbol{x}-\chi_i(t)) \tag{2}$$

where $\delta\chi_i(t)$ is the arc length increment associated with the ith element [4,8], δ is a *numerical* core radius, and $\kappa_\delta(\boldsymbol{x})$ is the velocity smoothing kernel. The numerical core radius δ is related to the physical core size σ in such a way that desingularized velocity field from equation (2) matches the asymptotic analytical prediction at the filament centerline [4,7].

As mentioned earlier, $\boldsymbol{v}^{\mathrm{out}}$ is the potential flow due to the presence of the sphere. The latter has been studied by Knio & Ting [2] who extend the classical results of Weiss [9] and Lighthill [10].

In particular, analytical formulas are provided in [2] for the "image" potential and the associated velocity field. These formulas express "image" velocity as a line integral along the image of the filament centerline with regular weight functions. Thus, the image velocity can be computed in a similar fashion to the self-induced velocity.

The far-field sound emission is estimated using the procedure of Ting & Miksis [11], which is based on matching the far-field acoustic potential to the potential induced by the slender filament and by its "image". This approach also leads analytical expressions of the far-field sound [1,2,7]. The latter show the interaction between the filament and the rigid sphere results in the generation of O(M) dipoles and O(M^2) quadrupoles, where M is the Mach number. The strengths and orientations are determined by the time evolution of the first and second moments of the filament vorticity and by *weighted* first and second moments of the "image".

In the computations below, the 3D filament scheme is used to compute the coaxial passage of a vortex ring over a sphere. The results are then compared to predictions obtained using an axisymmetric particle scheme, whose construction is highlighted below.

3 Particle Model

Lagrangian simulations are also performed using a particle method for axisymmetric viscous flow, whose construction is discussed in [6]. The method is based on discretization of the vorticity field into desingularized vortex elements and transport of these elements in a Lagrangian reference frame. The regularization is performed in a spatially non-homogenous fashion using specially tailored, spatially non-homogenous, core distribution functions; it is implemented so that conditions on the axis of symmetry are naturally satisfied. The element are advected using a local velocity vector which is expressed as the sum of (i) a vortex interaction velocity given in terms of a desingularized Biot-Savart law [21], (ii) a potential velocity expressed in terms of the image of vortex elements, and (iii) a diffusion velocity [6,12]. In the present work, attention is focused on inviscid flows so that the diffusion velocity is ignored.

Finally, we mention that the restriction to axisymmetric flow enables a simplified representation of the images of the vortex elements. In particular, one can immediately apply the classical result for the image of a coaxial vortex ring in a stationary rigid sphere [13]. The corresponding image representation is exploited in the present calculations.

4 Results and Discussion

The filament and particle schemes were used to analyze the effects of various parameters, including (a) the initial core to ring radius ratio, $\alpha \equiv \sigma_0/R_0$, (b) the ratio of initial ring radius to sphere radius, R_0/a, and (c) the Reynolds number. The particle computations were also used to examine the effect of the initial core vorticity distribution. For brevity, however, only a small subset of the computations is discussed; a more detailed account will be provided elsewhere [14,15].

Figure 1 shows the distribution of the particles at different times in the axisymmetric calculations. Shown in figure 1a are results for a thin ring with $\alpha = 0.1$; figure 1(b) shows similar results for a thicker ring with $\alpha = 0.3$. In both cases, the initial ring radius coincides with that of the sphere,

i.e. $R_0/a = 1$. Also plotted in figure 1 is the trajectory of the centroid of the core vorticity. Note that since the leading-order vorticity depends on the radius, the centroid of vorticity is close to, does not coincide with the geometric center of the core (figure 1b). The distinction between the two points is easier to appreciate when the core cross-section is larger.

The results indicate that as the vortex ring passes over the sphere, its radius stretches while its cross-section becomes thinner [16,17]. Due to their larger self-induced velocity, thin rings complete the passage in a shorter time period than thicker rings. As the core to radius ratio decreases the trajectory of the core centroid comes closer to the surface of the sphere [1]. The results also show that during the interaction with the sphere, the cross-section of the vortex core becomes deformed, as it acquires a predominantly elliptic shape with flat side facing the sphere surface. Following the interaction, the ring radius decreases towards its initial value, as can observed in figure 1; this reflects the non-diffusive nature of the Lagrangian calculations. However, the initial core vorticity distribution in the particle calculations is not recovered after the passage over the sphere. The deformation of the vortex core takes the form of a filamentation process which is amplified during the interaction. The process was clearly observed in vorticity contour plots (not shown), and may be appreciated by following the evolution of the particle distributions. It should be also be noted that the extent of the deformation of the vortex core and the stretching of the ring radius depend, in addition to the core to radius ratio, on other parameters, including the ratio of initial ring radius to sphere radius, and the assumed initial core vorticity distribution and the Reynolds number. For brevity, discussion of the effect of these parameters is omitted.

The particle predictions of vortex motion are contrasted with corresponding slender filament results in figures 2 and 3. Figure 2 compares the computed trajectories of the vortex core, while figure 3 contrasts results for the instantaneous velocity of the vortex core center. Both figures use results for a ring with $\alpha = 0.1$ and $R_0/a = 1$. The plots reveal a very favorable agreement between the slender filament and particle calculations. This is not surprising since the present ring/sphere parameters are well within the regime of validity of the slender filament model. The agreement between the trajectory and propagation velocity deteriorates only slightly as the core to radius ratio is increased. Thus, the deformation of the vortex core and the internal motion associated with filamentation does not appear to have a major impact on the global features of the vortex ring propagation.

The normalized far-field acoustic pressure for a passage with $\alpha = 0.1$, $R_0/a = 1$ and Mach number $M = 0.05$ is plotted in figure 4. Shown are results of the slender filament and particle simulations. Results for acoustic emission along the axis of propagation ($\theta = 0$) are given in figure 4a, and for emission normal to the ring axis ($\theta = 90^\circ$) in figure 4b. The figures show that the passage of the ring over the sphere results in the generation of an acoustic pressure spike, whose properties have been extensively discussed in [1] in light of slender filament computations. Meanwhile, the acoustic pressure signal computed in the particle simulation reveals a high frequency component that is not observed in the filament calculations. In fact, the acoustic signal in the particle simulation appears to be composed of a low-frequency component, whose evolution is in agreement with the signal from the slender vortex model, on which are superimposed high-frequency oscillations. Analysis of the computations indicates that the origin of the high frequency oscillations is due to unsteady, non-axisymmetric motion within the vortex core. Prior to the passage, the unsteady motion has a very small amplitude, since the particle calculations were initialized using the steady, asymptotic, constant-vorticity core distribution given by Fraenkel [18]. During the passage, the core vorticity is severely deformed (not shown) and a filamentation processes is induced. This triggers the high-frequency pressure emission whose characteristic period coincides with the rotation period within the core. Note that due to the destabilization of the vortex core, the high-frequency emission

persist even after the passage is completed. Analysis of the computations also reveals that the high-frequency acoustic pressure emission is quadrupolar in nature [19,20] and consequently scales with the square of the Mach number. Meanwhile, the emission generated by the interaction with the sphere is dominated by an O(M) dipole emission which, for the present setup, has a fixed directivity along the axis of the ring [1]. A somewhat high value of M has been selected in figure 4 in order to highlight the effect of the quadrupoles.
We are currently performing additional calculations in order to analyze the effect of different initial core vorticity distribution and the effect of viscosity on the evolution of the core and on the associated sound emission. These results will be discussed in a future study.

References

1 Knio, O.M., Ting, L., and Klein, R.: Interaction of a slender vortex with a rigid sphere: Dynamics and far-field sound, J. Acoust. Soc. Am. **103**, 83 (1998).
2 Knio, O.M. and Ting, L.: Vortical flow outside a sphere and sound generation. SIAM J. Appl. Math. **57**, 972 (1997).
3 Klein, R., Knio, O.M., and Ting, L.: Representation of core dynamics in slender vortex simulations. Phys. Fluids **8**, 2415 (1996).
4 Klein, R., and Knio, O.M.: Asymptotic vorticity structure and numerical simulation of slender vortex filaments. J. Fluid Mech. **284**, 275 (1995).
5 Callegari, A., and Ting, L.: Motion of a curved vortex filament with decaying core and axial velocity. SIAM J. Appl. Math. **15**, 148 (1978).
6 Rivoalen, E. and Huberson, S.: Numerical simultation of axisymmetric viscous flows by means of vortex particles method. Submitted to J. Comput. Phys. (1998).
7 Knio, O.M., and Ting, L.: Noise emission due to slender vortex solid body interactions. Proc. IUTAM Symposium on Dynamics of Slender Vortices, Kluwer, pp. 347-360 (1998).
8 Knio, O.M., and Ghoniem, A.F.: Numerical study of a three-dimensional vortex method. J. Comput. Phys. **86**, 75 (1990).
9 Weiss, P.: On hydrodynamical images–Arbitrary irrotational flow disturbed by a sphere. Proc. Cambridge Philos. Soc. **40**, 259 (1944).
10 Lighthill, M.J.: The image system of a vortex element in a rigid sphere. Proc. Cambridge Philos. Soc. **52**, 317 (1956).
11 Ting, L., and Miksis, M.J.: On vortical flow and sound generation. SIAM J. Appl. Math. **50**, 251 (1990).
12 Rivoalen, E., Huberson, S., and Hauville, F.: Numerical simulation of Navier-Stokes equations by means of the particle method. C. R. Acad. Sci. Paris Ser. IIb **324**, 543 (1997).
13 Lamb, H.: *Hydrodynamics*. Dover (1945).
14 Rivoalen, E., Huberson, S., and Knio, O.M.: Numerical study of sound radiation by an isolated vortex ring. In preparation.
15 Rivoalen, E., Huberson, S., and Knio, O.M.: Simulation of sound emission by the interaction of an axisymmetric vortex ring with a stationary rigid sphere. In preparation.
16 Wang, H.-C.: The motion of a vortex ring in the presence of a rigid sphere. Annual Report of the Institute of Physics, Academia Sinica, Taiwan, pp. 85–93 (1970).
17 Miyazaki, T., and Kambe, T.: Axisymmetric problem of vortex sound with solid boundaries. Phys. Fluids **29**, 4006 (1986).
18 Fraenkel, L.E.: On steady Vortex rings of small cross-section in an ideal fluid. J. Fluid Mech. **51**, 119 (1972).
19 Knio, O.M., and Juvé, D.: On noise emission during coaxial ring collision. C. R. Acad. Sci. Paris Ser. II **322**, 591 (1996).
20 Knio, O.M., Collorec, L., and Juvé, D.: Numerical Investigation of the Sound Emitted by 2D Regular and Chaotic Vortex Configurations. J. Comput. Phys. **116**, 226 (1995).
21 M. Nitsche: Axisymmetric vortex sheet roll-up. Ph.D Thesis, University of Michigan (1992).

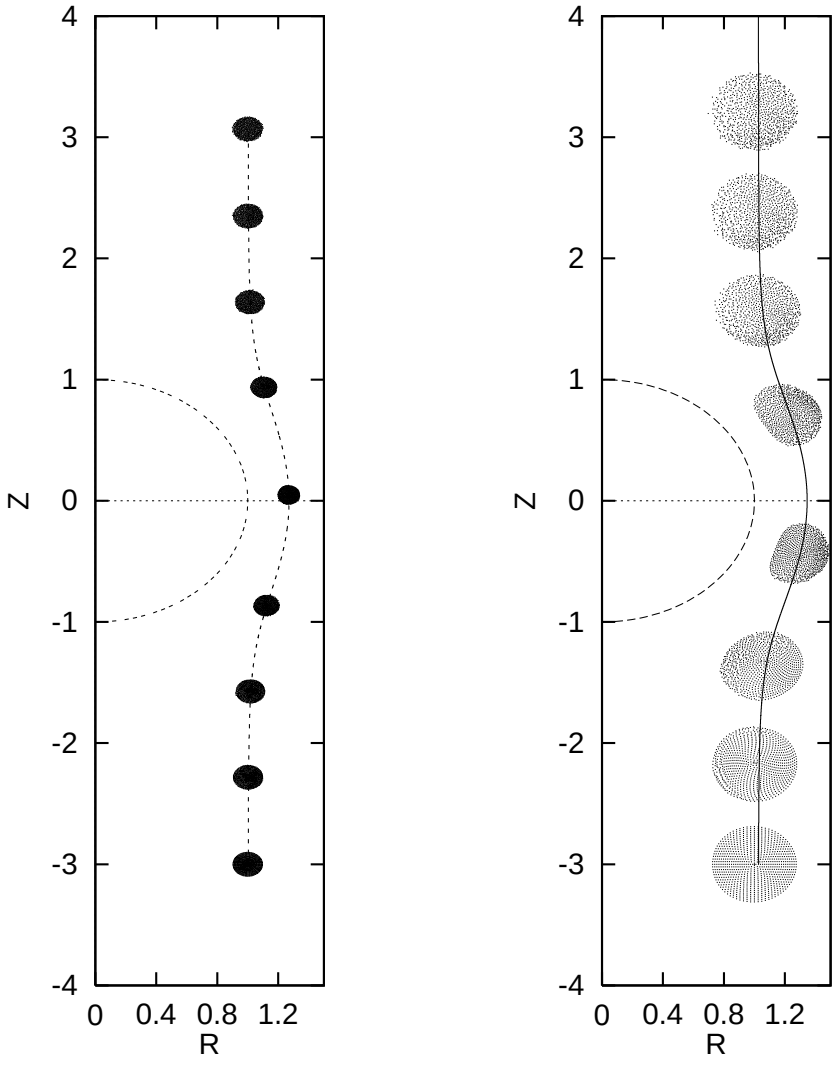

Figure 1: Position of the particles at different times. The core center is initially located $R = 1$, $Z = -3$. The core vorticity distribution is initially uniform ($\omega/r = C$) and its shape is taken from Fraenkel's solution. The core is discretized using 841 particles. The ring travels from bottom to top. (a) Thin ring with core to radius ratio $\alpha = 0.1$. The time step $\Delta t\Gamma/a^2 = 0.0045$, and the particles are plotted at times $t\Gamma/a^2 = 0$, 4.5, 9, 13.5 and 18. (b) Thick ring with core to radius ratio $\alpha = 0.3$. The the time step $\Delta t\Gamma/a^2 = 0.00705$, and the particles are plotted at times $t\Gamma/a^2 =$ 0, 3.53, 7.05, 10.58, 14.1, 17.63, 21.16 and 24.69.

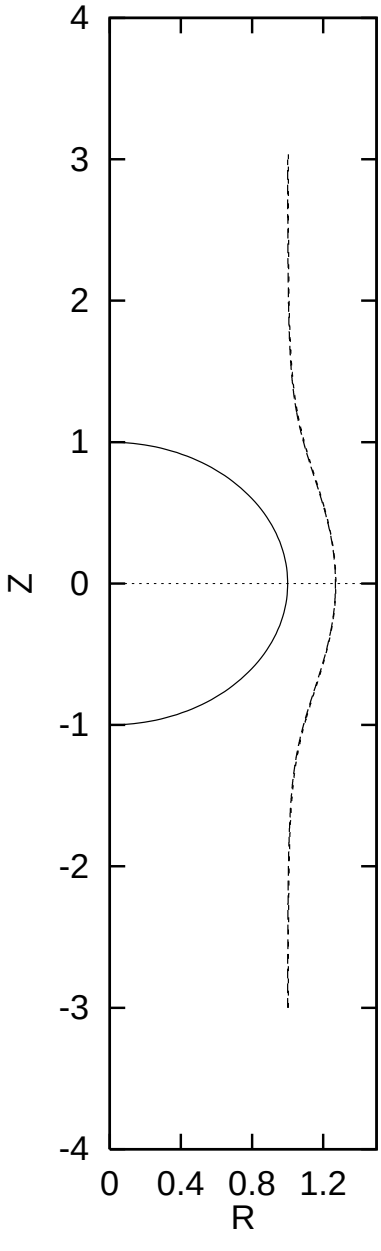

Figure 2: Trajectory of the center the vortex core for the ring of Fig. 1a: (—) slender filament model; (– – –) particle calculations.

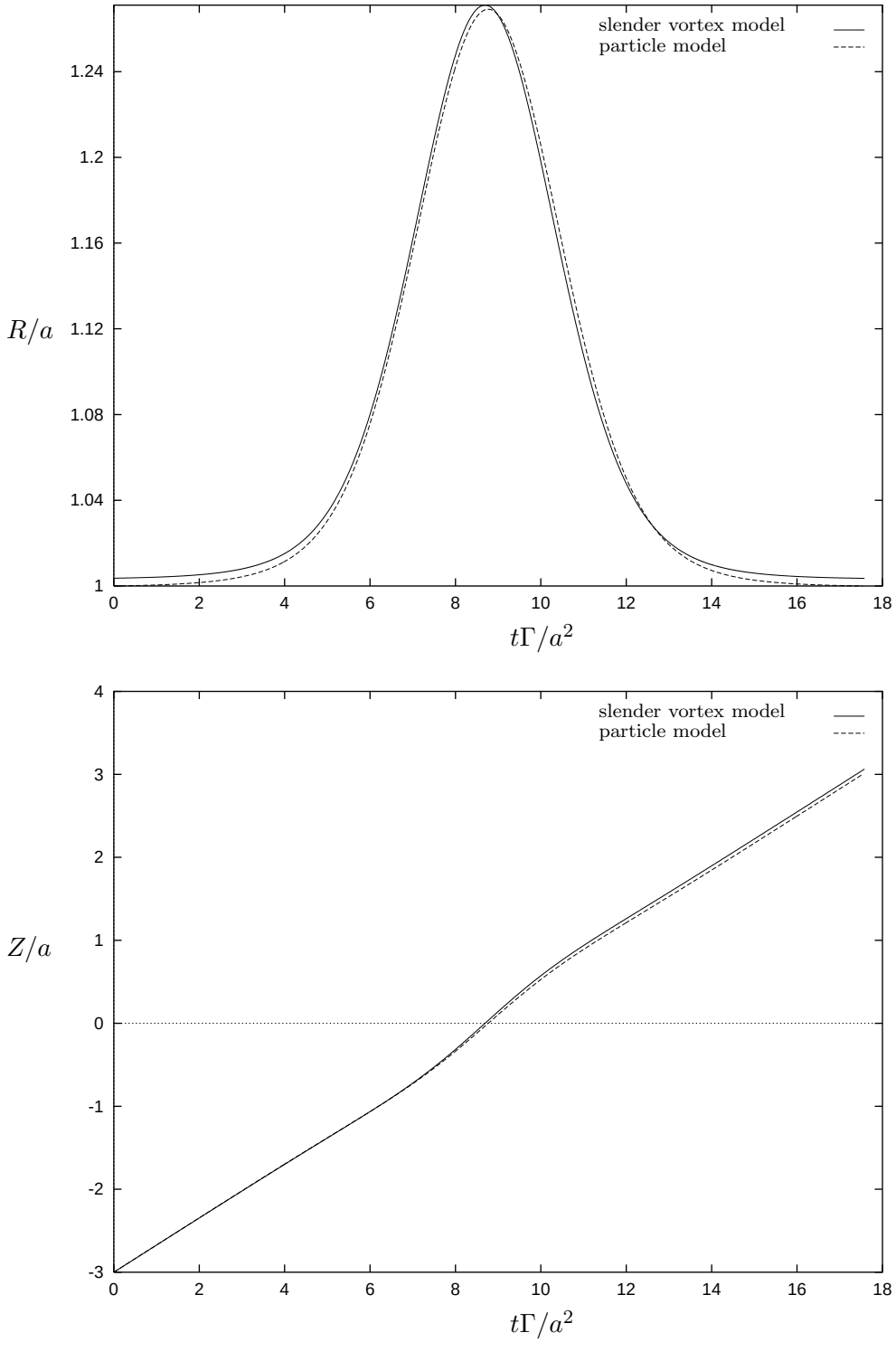

Figure 3: Evolution of the core position for the ring of Fig. 1a. Results of the filament model and the particle simulations are contrasted.

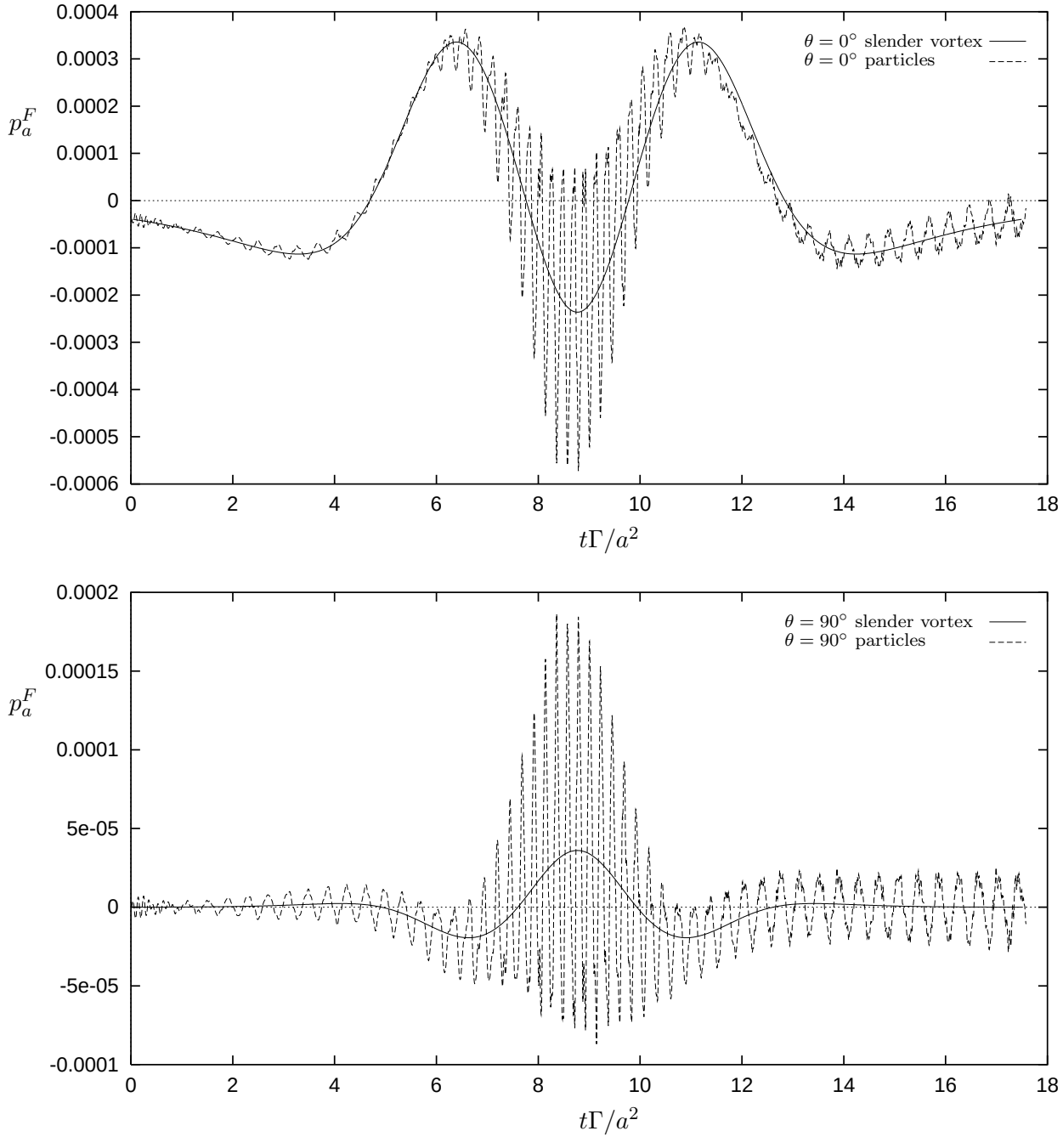

Figure 4: Far-field acoustic pressure for passage $R/a = 1$, $\alpha = 0.1$, and $M = 0.05$. Results of the filament model and the particle simulations are contrasted.